INTERNAL HEAT TRANSFER AUGMENTATION IN A CHANNEL USING AN ALTERNATE SET OF POROUS CAVITY-BLOCK OBSTACLES

P. C. Huang and K. Vafai
Department of Mechanical Engineering, Ohio State University, Columbus, Ohio, USA

A numerical investigation for forced convection in a constant-temperature parallel plate channel with porous cavity and block alternately emplaced on the bottom plate is presented in this work. The Brinkman-Forchheimer-extended Darcy model, which accounts for the effects of impermeable boundary and inertia, is used to characterize the flow field inside the porous region. Solutions of the coupled governing equations are carried out through the stream function–vorticity analysis. The characteristics of fluid flow and forced convection heat transfer have been obtained by the examinations of various governing parameters, such as the Reynolds number, Darcy number, inertial parameter, Prandtl number, and two geometric parameters. Several interesting phenomena such as the heat transfer augmentation in the channel were presented and discussed. The results of this investigation indicate that the size of recirculation caused by porous block will have a profound effect on the flow and heat transfer characteristics inside the interblock porous cavity.

The problem of convective heat transfer and fluid flow in horizontal ducts with fins and ribs has been well studied and documented because of the augmentation effect on the heat transfer process. The similar problem with a porous structure has also gained extensive attention due to the wide range of applications, which include, but are not restricted to, areas such as thermal insulation, crude oil extraction, solidification of castings, nuclear waste repositories, and solid matrix heat exchangers.

Shah and London [1] provided a comprehensive survey of literature pertinent to the heat transfer performance studies within a channel without a porous medium, while Koh and Colony [2] numerically investigated the cooling effectiveness for a porous material in a coolant passage. Koh and Stevens [3] performed an experimental study for the same problem. They showed for the case with fixed allowable wall temperature that the heat flux at the channel wall can be increased by over 3 times by using high-conductivity porous material in the channel. Rohsenow and Hartnett [4] presented the constant Nusselt number for the fully developed region in a porous medium bounded by two parallel plates, based on Darcy's flow model. To account for the effect of a solid boundary, Kaviany [5] performed a

Received 8 March 1993; accepted 7 May 1993.
The support of DOE under grant DE-FG02-93ER61612 for part of this work is acknowledged and appreciated.
Address correspondence to Dr. K. Vafai, Department of Mechanical Engineering, Ohio State University, 206 West 18th Avenue, Columbus, OH 43210-1107, USA.

Numerical Heat Transfer, Part A, 25:519–539, 1994

1040–7782/94 $10.00 + .00

NOMENCLATURE

A	dimensionless geometric parameter ($= W^*/H^*$)	Γ	general diffusive coefficient, Eq. (15)
B	dimensionless geometric parameter ($= D^*/W^*$)	δx	x direction distance between two adjacent grid points
D	spacing between cavities or blocks, m	δy	y direction distance between two adjacent grid points
Da	Darcy number ($= K/R^2$)	Δx	x direction width of the control volume
F	function used in expressing inertia terms	Δy	y direction width of the control volume
h	convective heat transfer coefficient, W/m^2 K	ϵ	porosity of the porous medium
H	height of the porous cavities or blocks, m	θ	dimensionless temperature $[= (T - T_0)/(T_w - T_0)]$
k	thermal conductivity, W/m K	Λ	inertial parameter ($= FR\epsilon/\sqrt{K}$)
K	permeability of the porous medium, m^2	μ	dynamic viscosity, kg/ms
l_1	length of plate upstream from the cavity-block array, m	ν	kinematic viscosity, m^2/s
l_2	length of plate downstream from the cavity-block array, m	ξ	vorticity
L	length of the parallel plate channel, as shown in Figure 1, m	Φ	transported property; general dependent variable
N	number of mixed porous cavity–block structures	ψ	stream function
Nu	Nusselt number ($= hx/k_f$)	$[a, b]$	larger of a and b
Pe	Péclet number ($= u_{av}R/\alpha$)		
Pr	Prandtl number ($= \nu/\alpha$)	**Superscript**	
R	height of channel	*	dimensionless quantity
Re	Reynolds number ($= u_{av}R/\nu$)	**Subscripts**	
T	temperature, K		
u	x component velocity, m/s	av	average
v	y component velocity, m/s	eff	effective
v	velocity vector, m/s	f	fluid
W	width of the porous block, m	I	interface
x	horizontal coordinate, m	m	bulk mean
y	vertical coordinate, m	p	porous
α	thermal diffusivity, m^2/s	x	local
α_{eff}	effective thermal diffusivity ($= k_{eff}/\rho_f c_{p,f}$), m^2/s	w	wall
		0	condition at inlet

numerical study of laminar flow through a porous medium bounded by isothermal plates based on the Brinkman-extended Darcy model for constant porosity. Poulikakos and Renken [6] have examined the effect of flow inertia, variable porosity, and a solid boundary on forced convection in a duct filled with porous media.

An important problem related to forced convection through a porous medium is flow and heat transfer over a porous/fluid composite system. This involves the study of fluid flow above and through a porous medium. Under this circumstance, the porous/fluid interfacial region represents a zone of discontinuity of material

properties. It has a direct influence on the fluid flow and heat transfer, especially when there is a large gradient of physical properties such as permeability, porosity, and thermal conductivity, across the interface. This type of composite system is encountered in many cases of practical interest, such as nuclear waste repositories, crude oil extraction, and iron blast furnaces. There exists an extensive work [7], which describes coupled fluid motions satisfying the Navier-Stokes equations in the free fluid, empirical, or semiempirical set of equations (typically, Darcy's law) in the permeable material, and matching conditions at the interfacial boundaries.

Beavers and Joseph [8] experimentally reported the mass efflux of a Poiseuille flow over a naturally permeable boundary based on Darcy's law. They found that when a viscous fluid passes a porous solid, tangential stress entrains the fluid below the interface with a velocity that is slightly greater than that of the fluid in the bulk of the porous medium. Both experimental and theoretical investigations for validating such slip-flow interface conditions were done by Taylor [9] and Richardson [10]. Levy and Sanchez-Palencia [11] found that when the typical length scale of the external flow is large compared with the microscopic scale, the velocity field transition at the interface from the porous media to the free-fluid region occurs over a thin region of the order of the pore scale. They also showed that, depending on the direction of the pressure gradient in the porous medium, two different kinds of phenomena may appear at the interface.

Recently, Vafai and Thiyagaraja [12] analytically studied a general class of problems involving interactions on flow and heat transfer for three basic types of interface zones. They obtained analytical solutions for the velocity and temperature distributions as well as analytical expressions for the Nusselt numbers for all three classes of interface composites investigated in their work. More relevant to the present study is the work of Poulikakos and Kazmierczak [13]. They analyzed fully developed forced convection in a channel partially filled with a porous matrix and showed that a critical thickness exists at which the value of Nusselt number reaches a minimum, based on the Brinkman-extended Darcy model.

Analysis of internal forced convection in a porous/fluid composite system is significantly more complicated due to the complex geometric configuration of these types of systems. In this study, a numerical investigation has been performed for a channel, within which multiple porous cavity and block structures are alternately emplaced. The analysis is based on the use of the Brinkman-Forchheimer-extended Darcy model in the porous medium and the Navier-Stokes equation in the fluid region. The porous medium provides a penetrating random structure, which augments the mixing in the fluid and profoundly changes the heat transfer characteristics within the channel. Therefore, the present study is aimed at a fundamental investigation of changes in the flow pattern and heat transfer performance due to the existence of porous cavity–block obstacles. Effects of various governing physical parameters are also considered in order to investigate their influence on the flow and thermal characteristics within the channel.

THEORY

The problem consists of flow between parallel plates with a multiple porous cavity–block structure on the bottom boundary, as depicted in Figure 1*a*. The fluid

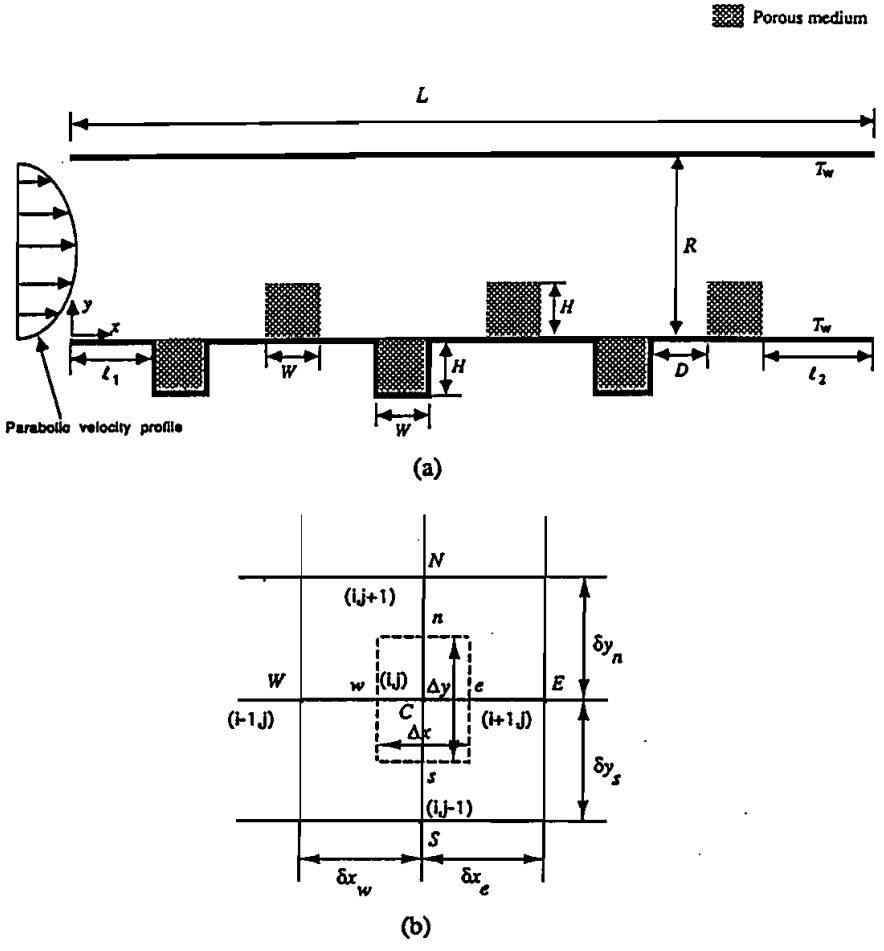

Figure 1. (a) Schematic diagram of force convection in a parallel plate channel with alternate porous cavity–block obstacles on the bottom plate. (b) Local integration cell.

enters the channel at ambient temperature T_0. It is assumed that the hydrodynamic entry length is small, resulting in a parabolic velocity profile at the entry to the channel. Alternatively, this parabolic velocity profile can also occur for a regular channel entrance region prior to the region of multiple porous cavity–block structures. The plate walls are maintained at constant temperature T_w, the channel width and total length are R and L, and the width and height of the rectangular porous cavities and blocks are H and W, respectively. The distance between cavity and block is designated as D, and the length of the plate upstream and downstream from the porous cavity–blocks are l_1 and l_2, respectively The flow is assumed to be steady, incompressible, and two-dimensional. In addition, the thermophysical properties of the fluid and the porous matrix are assumed to be constant, and the porous medium is considered homogeneous, isotropic, nondeformable, and in local thermodynamic equilibrium with the fluid. In this study, the

Brinkman-Forchheimer-extended Darcy model, which accounts for the effects of flow inertia as well as friction caused by macroscopic shear [14, 15], is used to describe the flow inside the porous regions. This work is based on the application of an efficient method combining the two sets of governing equations for the fluid and the porous regions into one set of conservation equations satisfying the matching conditions at the porous/fluid interface. The resulting momentum and energy equations in terms of dimensionless variables are as follows:

$$\frac{\partial \psi^*}{\partial y^*}\frac{\partial \xi^*}{\partial x^*} - \frac{\partial \psi^*}{\partial x^*}\frac{\partial \xi^*}{\partial y^*} = \frac{1}{\mathrm{Re}}\nabla^2 \xi^* + S^* \tag{1}$$

$$\nabla^2 \psi^* = -\xi^* \tag{2}$$

$$\frac{\partial \psi^*}{\partial y^*}\frac{\partial \theta}{\partial x^*} - \frac{\partial \psi^*}{\partial x^*}\frac{\partial \theta}{\partial y^*} = \nabla\left(\frac{1}{\mathrm{Pe}}\nabla\theta\right) \tag{3}$$

The nondimensional parameters in the fluid region are

$$\mathrm{Re} = \frac{u_{\mathrm{av}} R}{\nu_f} \qquad \mathrm{Pe} = \frac{u_{\mathrm{av}} R}{\alpha_f} \qquad S^* = 0 \tag{4}$$

and the nondimensional parameters in the porous region are

$$\mathrm{Pe} = \frac{u_{\mathrm{av}} R}{\alpha_{\mathrm{eff}}} \qquad \mathrm{Da} = \frac{K}{R^2} \qquad \Lambda = \frac{FR\epsilon}{K^{1/2}} \tag{5}$$

$$S^* = -\frac{1}{\mathrm{Re\,Da}}\xi^* - \Lambda|\mathbf{v}^*|\xi^* - \Lambda\left(v^*\frac{\partial|\mathbf{v}^*|}{\partial x} - u^*\frac{\partial|\mathbf{v}^*|}{\partial y^*}\right) \tag{6}$$

where the nondimensional quantities are

$$x^* = \frac{x}{R} \qquad y^* = \frac{y}{R} \qquad u^* = \frac{u^*}{u_{\mathrm{av}}} \qquad v^* = \frac{v}{u_{\mathrm{av}}} \qquad |\mathbf{v}^*| = \sqrt{u^{*2} + v^{*2}} \tag{7}$$

$$\psi^* = \frac{\psi}{u_{\mathrm{av}} R} \qquad \xi^* = \frac{R\psi}{u_{\mathrm{av}}} \qquad \theta = \frac{T - T_0}{T_{\mathrm{w}} - T_0} \tag{8}$$

The source term S^* in the porous region is composed of those terms contributing to the vorticity generation due to the presence of the porous medium. In addition, the above stream function and vorticity are defined as

$$u = \frac{\partial \psi}{\partial y} \qquad v = -\frac{\partial \psi}{\partial x} \tag{9}$$

$$\xi = \frac{\partial v}{\partial x} - \frac{\partial u}{\partial y} \tag{10}$$

It should be noted that the variables v and T in the porous regions are both volume-average quantities, as described by Vafai and Tien [14].

BOUNDARY CONDITIONS

Due to the elliptic nature of the conservation equations, the boundary conditions for all field variables have to be specified along the entire boundary enclosing the solution domain. At the inlet of the channel, the stream function distribution is calculated from the specified inlet fluid velocity profile, that is, a fully developed parabolic profile. At the outlet, the gradient of the stream function in the axial direction is assumed to be zero; i.e., the streamlines are assumed to be perpendicular to the exit plane of the channel. This boundary condition frequently appears in the literature [16] and implies that the flow is almost fully developed at the exit. Even though the fully developed flow may not be achieved at the exit of the channel, this zero-gradient boundary condition offers sufficient flexibility for the flow distribution. Furthermore, by choosing an extended computational domain, it was ensured that the outflow boundary conditions had no detectable effect on the solution within the physical domain. This process is explained in more detail below.

The vorticity boundary conditions are derived from the velocity distribution. For the thermal boundary conditions, the fluid is assumed to have a uniform temperature distribution at the inlet, while at the outlet the temperature gradient along the flow direction is taken to be negligible, indicating that the convective effects are taken to be more dominant than the diffusion of heat. Again, by choosing an extended computational domain, it was ensured that the thermal boundary conditions at the exit had no significant effect on the solution. For closure, the matching conditions, which satisfy the continuity of longitudinal and transverse velocities, normal and shear stresses, temperature, pressure, and heat fluxes, are applied across the porous/fluid interfaces [17, 18]. In summary, the boundary conditions can be described in the following dimensionless form.

1. At the entrance ($x^* = 0, 0 < y^* < 1$),

$$u^* = 6y^*(1 - y^*) \qquad v^* = 0 \qquad \psi^* = 6\left(\frac{y^{*2}}{2} - \frac{y^{*3}}{3}\right)$$

$$\xi^* = 6(1 - 2y^*) \qquad \theta = 0$$

2. At the exit ($x^* = L^*, 0 < y^* < 1$),

$$\int_0^1 u^* \, dy^* = 1 \qquad v^* = 0$$

$$\frac{\partial \psi^*}{\partial x^*} = 0 \qquad \frac{\partial \theta}{\partial x^*} = 0$$

3. Along the bottom plate,

$$0 < x^* < l_1^*$$

$$l_1^* + NW^* + 2(N-1)(W^* + D^*) < x^* < l_1^* + NW^* + N(W^* + 2D^*)$$

$$(1 - l_2^*) < x^* < 1$$

(all at $y^* = 0$) and on the cavity floor,

$$l_1^* + 2(N-1)(W^* + D^*) < x^* < l_1^* + W^* + 2(N-1)(W^* + D^*)$$

$$y^* = -H^*$$

the following boundary conditions are applied:

$$u^* = 0 \qquad v^* = 0 \qquad \psi^* = 0$$

$$\xi^* = -\frac{\partial^2 \psi^*}{\partial y^{*2}} \qquad \theta = 1$$

4. Along the upper plate ($0 < x^* < L^*$, $y^* = 1$),

$$u^* = 0 \qquad v^* = 0 \qquad \psi^* = 1$$

$$\xi^* = -\frac{\partial^2 \psi^*}{\partial y^{*2}} \qquad \theta = 1$$

5. Along the side walls of the cavities,

$$x^* = l_1^* + 2(N-1)(W^* + D^*)$$

$$x^* = l_1^* + W^* + 2(N-1)(W^* + D^*) \qquad 0 > y^* > -H^*$$

$$u^* = 0 \qquad v^* = 0 \qquad \psi^* = 0$$

$$\xi^* = -\frac{\partial^2 \psi^*}{\partial x^{*2}} \qquad \theta = 1$$

6. Along the porous/fluid interface,

$$u_f^* = u_p^* \qquad v_f^* = v_p^*$$

$$\mu_f \frac{\partial v_f^*}{\partial y^*} = \mu_{eff} \frac{\partial v_p^*}{\partial y^*} \qquad \mu_f \left(\frac{\partial u_f^*}{\partial y^*} + \frac{\partial v_f^*}{\partial x^*} \right) = \mu_{eff} \left(\frac{\partial u_p^*}{\partial y^*} + \frac{\partial v_p^*}{\partial x^*} \right)$$

$$\theta_f = \theta_p \qquad k_f \frac{\partial \theta_f}{\partial x^*} = k_{eff} \frac{\partial \theta_p}{\partial x^*}$$

The parameter N $(= 1, 2, \ldots)$ is the number of mixed porous cavity–block obstacles. Note that the variables in the above equations are defined as follows:

$$L^* = \frac{L}{R} \qquad l_1^* = \frac{l_1}{R} \qquad l_2^* = \frac{l_2}{R} \qquad D^* = \frac{D}{R} \qquad W^* = \frac{W}{R}$$

From the above equations, boundary conditions, and geometry arrangement of porous cavities and blocks, it is seen that the present problem is governed by six dimensionless parameters. These are the Darcy, Reynolds, and Prandtl numbers, inertia parameter, and geometric parameters A and B, where

$$A = \frac{W^*}{H^*} \qquad B = \frac{D^*}{W^*} \qquad H^* = \frac{H}{R}$$

Further insight into the porous cavity–block interactions on the fluid flow and heat transfer processes can be obtained by observing the variation of the local heat transfer rates on the channel wall. The local Nusselt number along the bottom plate may be defined from the local heat transfer coefficient as

$$\mathrm{Nu}_x = \frac{hR}{k_f} = -\frac{k_{\mathrm{eff}}(T_w - T_0)}{k_f(T_w - T_m)} \left.\frac{\partial\theta}{\partial y^*}\right|_{y^*=0} = -\frac{k_{\mathrm{eff}}}{k_f} \frac{1}{(1-\theta_m)} \left.\frac{\partial\theta}{\partial y^*}\right|_{y^*=0} \tag{11}$$

where k_{eff} reverts to k_f over regions with no porous substrate and $\theta_m = (T_m - T_0)/(T_w - T_0)$ is the dimensionless form of the bulk mean temperature T_m defined by

$$T_m = \frac{\int_0^R |u| T \, dy}{\int_0^R |u| \, dy} \tag{12}$$

The absolute value of the velocity proposed by Kelkard and Patankar [19] is used here, so as to properly account for regions of recirculating flow. It should be noted that conductivity of the fluid was chosen in the formulation of Nu. This choice gives a more meaningful comparison for the heat flux at the channel between the composite system and the case where there was no porous substrate. Therefore, the heat transfer augmentation will be even larger for a porous medium that has a larger thermal conductivity than that of the fluid.

NUMERICAL METHOD

The following is a general formulation for the diffusion-convection equation, which can be applied to vorticity and temperature equations:

$$\frac{\partial}{\partial x}(u\Phi) + \frac{\partial}{\partial y}(v\Phi) = \frac{\partial}{\partial x}\left(\Gamma \frac{\partial \Phi}{\partial x}\right) + \frac{\partial}{\partial y}\left(\Gamma \frac{\partial \Phi}{\partial y}\right) + S^{\Phi} \tag{13}$$

Here, Φ represents either the temperature or vorticity function. The stream function equation Eq. (2) is solved using the successive overrelaxation (SOR) method. By using finite difference approximations, the governing equations can be reduced to a set of nonlinear algebraic equations that can be solved by an iteration scheme. Based on the nonuniform rectangular grid system, the finite difference form of the vorticity and temperature equations is derived by volume integration over discrete cells surrounding the grid points, as shown in Figure 1*b*. Calculations were performed using the second upwind-differencing scheme for the convective terms with central difference for the diffusive terms. This integration process results in a discretized equation that can be put into the form

$$C_C\Phi_{i,j} = C_E\Phi_{i+1,j} + C_W\Phi_{i-1,j} + C_N\Phi_{i,j+1} + C_S\Phi_{i,j-1} + b \tag{14}$$

where

$$C_E = \Gamma_e\frac{\Delta y}{\delta x_e}\left(1 + \left[-\frac{\delta x_e u_e}{\Gamma_e}, 0\right]\right) \tag{15a}$$

$$C_\omega = \Gamma_\omega\frac{\Delta y}{\delta x_\omega}\left(1 + \left[-\frac{\delta x_\omega u_\omega}{\Gamma_\omega}, 0\right]\right) \tag{15b}$$

$$C_N = \Gamma_n\frac{\Delta x}{\delta y_n}\left(1 + \left[-\frac{\delta y_n v_n}{\Gamma_n}, 0\right]\right) \tag{15c}$$

$$C_S = \Gamma_s\frac{\Delta x}{\delta y_s}\left(1 + \left[\frac{\delta y_s v_s}{\Gamma_s}, 0\right]\right) \tag{15d}$$

$$b = S^\Phi \Delta x\,\Delta y \tag{15e}$$

and

$$C_C = C_E + C_W + C_N + C_S \tag{15f}$$

The finite difference equations for ξ^* and θ obtained in this manner were solved by the extrapolated Jacobi scheme. This iterative scheme is based on a double cyclic routine, which translates into a sweep of only half of the grid points at each iteration step [20]. The numerical procedure for solving the finite difference equations is as follows:

1. Overlay the computational domain with a finite difference mesh.
2. Assign values of Re, Da, Λ, A, B, and N; initialize values for ξ^*, $\psi^* u$, v, and θ in Eqs. (1)–(6); and set boundary conditions.
3. Calculate the new values of vorticity ξ^* at each node by using Eq. (14) for ξ^*.
4. Calculate the new values of stream function ψ^* at each node using the SOR method and utilizing the obtained values of ξ^* from step 3.
5. Calculate the new values of the velocity from $u = \psi_y^*$ and $v = -\psi_x^*$.

6. Update new boundary values using the new nodal values of ψ^* and ξ^*.
7. Repeat steps 3–6, until the criterion of convergence for ξ^* and ψ^* is satisfied.
8. Calculate the temperature θ from Eq. (14) for the ψ^* values obtained from step 7 until the criterion of convergence for θ is satisfied.

Here, the following convergence criterion is used in these iterative procedures:

$$\max \left| \frac{\varphi_{i,j}^{n+1} - \varphi_{i,j}^{n}}{\varphi_{i,j}^{n}} \right| < 10^{-6} \tag{16}$$

where φ stands for ξ^*, ψ^*, or θ and n denotes the iteration number.

In the present numerical calculation of coupled elliptic governing equations with an extended computational boundary condition downstream of the channel, as explained previously, it is necessary to artificially specify the exit boundary location. The suitable location was chosen by trial and error to ensure that the recirculation zone was inside of the computational domain. Therefore, by choosing an extended computational domain, it was ensured that the computational outflow boundary condition had no effect on the physical domain solution.

A nonuniform mesh system with very fine grid spacing in regions of steep gradients, such as those close to the wall, corners, and blocks, was selected to obtain accurate vorticity, streamline, and isotherm distributions. We employed a proper combination of Δx and Δy to assure stability. This was done by a systematic decrease in the grid size until further refinement of the grid size showed no more than a 1% difference in the convergent result. The choice of 105 grid points in the y direction and 250 points in the x direction was found to provide grid independence for most of our results.

In order to obtain the vorticity at the wall, the assumption of the linear variation of vorticity from the wall to the neighboring point was used [16], that is,

$$\xi_p^* = -\left(\frac{3(\psi_{np}^* - \psi_p^*)}{\Delta y_{np}^2} + \frac{\xi_{np}^*}{2} \right)$$

where p denotes the boundary node and Δy_{np} is the spatial interval in the direction normal to the boundary. The vorticity at sharp corners requires special consideration. Here, average treatment for the evaluation of vorticity suggested by Greenspan [21] was applied to model the mathematical limit of a sharp corner as appropriately as possible.

To ensure the continuity of the diffusive and convective fluxes across the porous/fluid interface, the harmonic mean formulation suggested by Patankar [22] was employed to handle the abrupt changes in thermophysical properties, such as the permeability and thermal conductivity, across the interface. All of these effects on the interface are summarized in the nondimensional parameters Da, Λ, and Pr. For the present case, Da, Λ, and Pr at the interface of a control volume are as

follows:

$$\mathrm{Da}_{\mathrm{I}} = \frac{2\mathrm{Da}_{\mathrm{eff}}\,\mathrm{Da}_{\mathrm{f}}}{\mathrm{Da}_{\mathrm{eff}} + \mathrm{Da}_{\mathrm{f}}} \qquad \Lambda_{\mathrm{I}} = \frac{2\Lambda_{\mathrm{eff}}\Lambda_{\mathrm{f}}}{\Lambda_{\mathrm{eff}} + \Lambda_{\mathrm{f}}} \qquad \mathrm{Pr}_{\mathrm{I}} = \frac{2\mathrm{Pr}_{\mathrm{eff}}\,\mathrm{Pr}_{\mathrm{f}}}{\mathrm{Pr}_{\mathrm{eff}} + \mathrm{Pr}_{\mathrm{f}}} \tag{17}$$

Therefore, instead of the source terms in Eqs. (4) and (6), the following parameters were used across the interface: In the fluid side of the interface,

$$S^* = \frac{u^*}{\mathrm{Re}}\frac{\partial}{\partial y^*}\left(\frac{1}{\mathrm{Da}_{\mathrm{I}}}\right) - \frac{v^*}{\mathrm{Re}}\frac{\partial}{\partial x^*}\left(\frac{1}{\mathrm{Da}}\right) + |\mathbf{v}^*|u^*\frac{\partial\Lambda}{\partial y^*} - |\mathbf{v}^*|v^*\frac{\partial\Lambda}{\partial x^*} \tag{18a}$$

and in the porous side of the interface,

$$S^* = -\frac{1}{\mathrm{Re}\,\mathrm{Da}}\xi^* - \Lambda|\mathbf{v}^*|\xi^* - \Lambda\left(v^*\frac{\partial|\mathbf{v}^*|}{\partial x^*} - u^*\frac{\partial|\mathbf{v}^*|}{\partial y^*}\right)$$
$$+ \frac{u^*}{\mathrm{Re}}\frac{\partial}{\partial y^*}\left(\frac{1}{\mathrm{Da}}\right) - \frac{v^*}{\mathrm{Re}}\frac{\partial}{\partial x^*}\left(\frac{1}{\mathrm{Da}}\right) + |v^*|u^*\frac{\partial\Lambda}{\partial y^*} - |v^*|v^*\frac{\partial\Lambda}{\partial y^*} \tag{18b}$$

In addition, to accommodate the solution of the transport equations in both the fluid and porous regions, the effective viscosity of the fluid-saturated porous medium is set to be equal to the viscosity of fluid. It has been found that this approximation provides good agreement with experimental data [23, 24]. Note that at any time, constant values of Da and Λ for a specified porous substrate were used.

The mathematical model and the numerical scheme were checked by comparing the results obtained from the present numerical results with other relevant limiting cases available in the literature. The relevant studies for our case correspond to the problem of hydrodynamically fully developed forced convection in a channel partially filled with a porous medium on the wall [13], and external forced convection over a flat plate embedded in a porous medium (i.e., $H^* \to \infty$ and $W^* \to \infty$, representing the full porous medium case [12]. The result of these comparisons (being similar to those presented by Vafai and Kim [17]) showed that the numerical model predicts quite accurately the velocity and temperature fields in a porous/fluid composite system.

RESULTS AND DISCUSSION

The fixed input parameters that were used in all the simulations were $R = 1$, $l_1 = 13$, and $k_{\mathrm{eff}}/k_{\mathrm{f}} = 1.0$. To demonstrate the flow and temperature fields, only the portion concentrating on the porous/fluid region and its close vicinity is presented. Furthermore, for the sake of brevity, only the main features and characteristics of some of the results are discussed, and the corresponding figures are not presented. However, it should be noted that the computational domain includes a larger region than what is displayed in the subsequent figures.

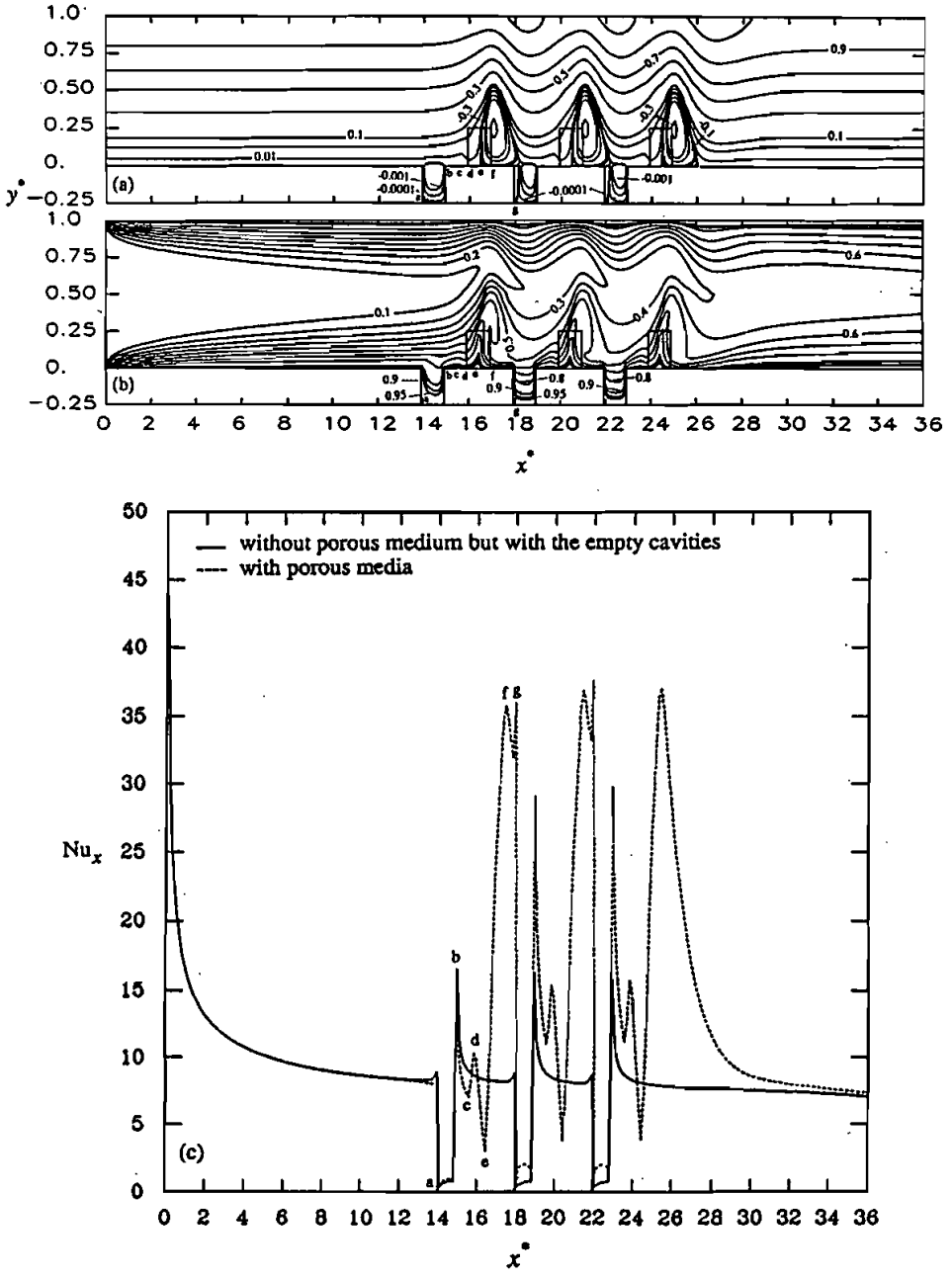

Figure 2. (a) Streamlines, (b) isotherms, and (c) local Nusselt number distribution for flow in a parallel plate channel with alternate-porous cavity–block obstacles on the bottom plate for Re = 750, Da = 3×10^{-5}, $\Lambda = 0.35$, Pr = 0.7, $k_{eff}/k_f = 1.0$ $A = 4$, $B = 1$, $H^* = 0.25$.

The effects of the porous cavity–block obstacles on the flow and temperature fields are illustrated in Figure 2 for a typical case. For the case shown in Figure 2, Re = 750, Da = 3×10^{-5}, the inertia parameter is 0.7, the dimensionless height and width of the porous cavity and block are 0.25 and 1.0, respectively, and the spacing between the porous cavities and the blocks is 1. It can be seen from Figure 2*a* that the presence of porous cavity–block obstacles causes the flow to bend significantly and to detach from the wall surface, forming a recirculation region behind each porous block. Small eddies are generated on the smooth upper plate surface corresponding to the reattached region on the bottom plate. However, even though the local behavior of flow adjacent to the porous cavity–block obstacles is affected by the existence of porous obstacles, flow somewhat downstream of the porous obstacles is not influenced at all. Here, the mechanism for the formation of recirculation regions in the rear part of the porous block is due to the relatively larger resistance that the flow encounters inside the porous block, which in turn displaces the flow by inducing a blowing effect from the porous region into the fluid region. Shortly after the porous block, the blowing effect disappears. Instead, the longitudinal pressure gradient, caused by the pressure drop behind the porous block, creates a suction effect that moves the flow downward to the space between the porous blocks. The flow patterns, including the shape of the recirculation zone, and the interactions between vortex flow inside the cavities and the external

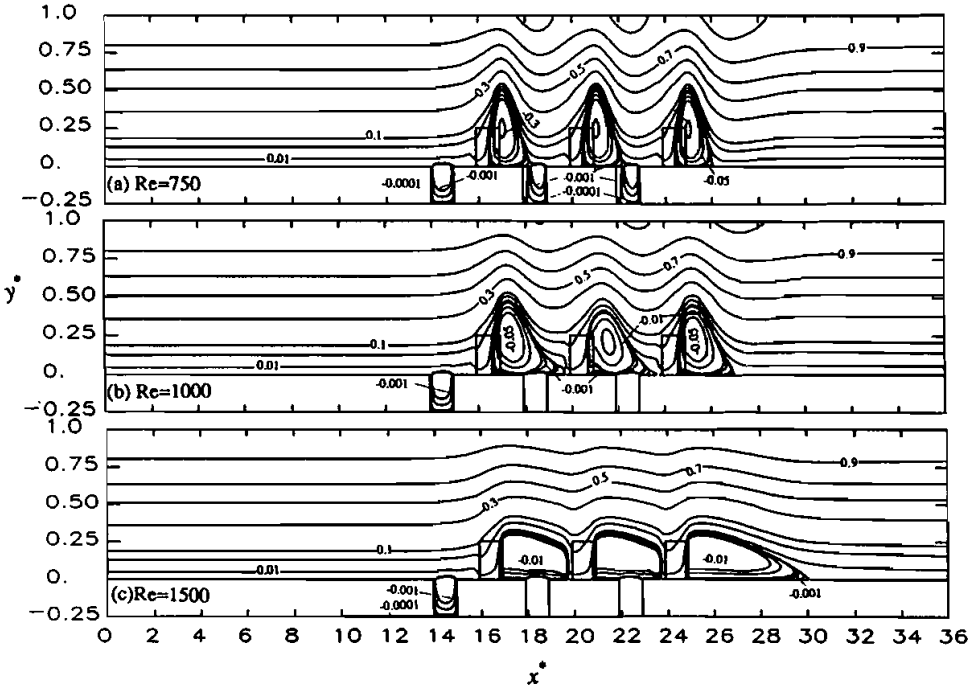

Figure 3. Effects of Reynolds number on streamlines for flow in a parallel plate channel with alternate porous cavity–block obstacles on the bottom plate for Da = 3×10^{-5}, $\Lambda = 0.35$, $A = 4$, $B = 1$, $H^* = 0.25$.

circulating flow play a significant role in affecting the temperature field. Figure 2*b* shows the isotherms corresponding to the above flow field.

It can be seen that the thickness of both the upper and lower thermal boundary layers increases along the length of the heated plates. These thermal boundary layers become considerably distorted around the porous obstacle regions. Shortly downstream of the porous cavity–block obstacles, the symmetrical character of the temperature field recurs. It should be noted that compared with the case without porous blocks in the channel, both upper and lower thermal boundary layers meet earlier due to the presence of porous blocks, which, as explained earlier, pushes the flow near the bottom plate upward.

The variation of local Nusselt number corresponding to the flow field shown in Figure 2*a* is depicted in Figure 2*c*. It should be noted that the case without the porous medium is for the channel that still includes the empty cavities. This way, the effects of the porous medium in enhancing the heat transfer from empty cavities is also illustrated in this work. In general, an empty cavity creates a close vortex region and reduces the heat transfer rate from the heated wall (the trough at point a in Figure 2*c*), while a porous block produces recirculating flow, which

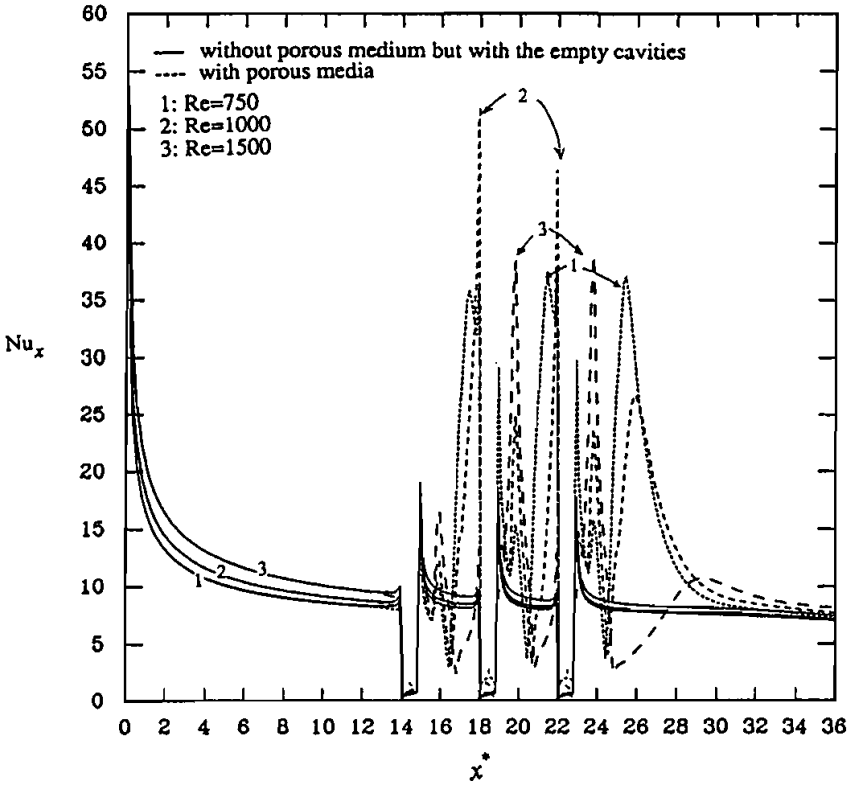

Figure 4. Effects of Reynolds number on local Nusselt number distribution for flow in a parallel plate channel with alternate porous cavity–block obstacles on the bottom plate for Da = 3×10^{-5}, $\Lambda = 0.35$, Pr = 0.7, $k_{eff}/k_{ff} = 1.0$, $A = 4$, $B = 1$, $H^* = 0.25$.

improves fluid mixing, resulting in a heat transfer augmentation (the peak at point f). In addition, the interaction between the circulation behind the porous blocks and the vortex inside the porous cavities can result in another heat transfer augmentation (the peak at point g). Similarly, other fluctuations in the Nu distribution are the result of various separations and reattachments occurring around the porous cavity–block region.

Effects of the Reynolds number. Figures 3 and 4 show the effect of the Reynolds number on the flow and temperature fields for Da = 3×10^{-5}, $\Lambda = 0.35$, Pr = 0.7, $A = 4$, $B = 1$, and $N = 3$, for Re = 750, 1000, and 1500. Comparison of the streamlines in Figure 3 shows that, as Re increases, the relative strength of the recirculation zone decreases while its lateral size increases. The recirculation zone thus occupies the whole interblock spacing, which reduces the interaction between the vortex inside the cavity and the closest recirculation zone. The reason for this trend is that increasing Re increases the fluid's momentum, resulting in a larger penetration into the porous blocks. This, in turn, increases the required length before reattachment occurs. Comparison of the isotherms indicates that as Re increases, the isotherms in the channel region become less distorted. Also as a result of the above-described flow field, the thermal penetration into each of the cavities that are followed by a porous block is reduced.

The variation of local Nusselt number for various Re is displayed in Figure 4. Again, it should be noted that the case without the porous medium is for the

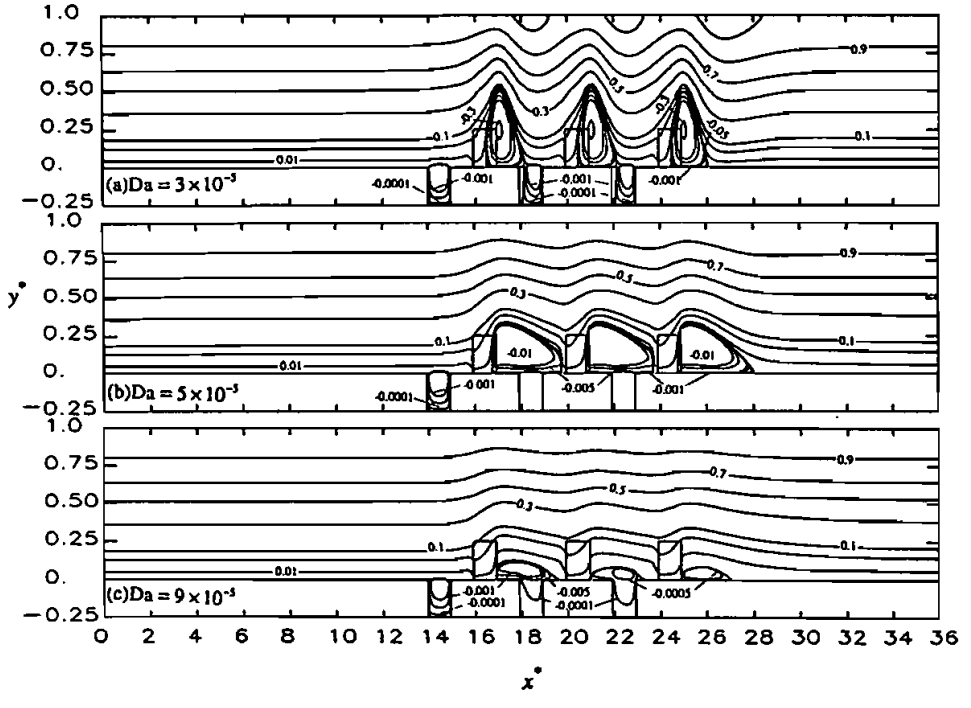

Figure 5. Effects of Darcy number on streamlines for flow in a parallel plate channel with alternate porous cavity–block obstacles on the bottom plate for Re = 750, $\Lambda = 0.35$, $A = 4$, $B = 1$, $H^* = 0.25$.

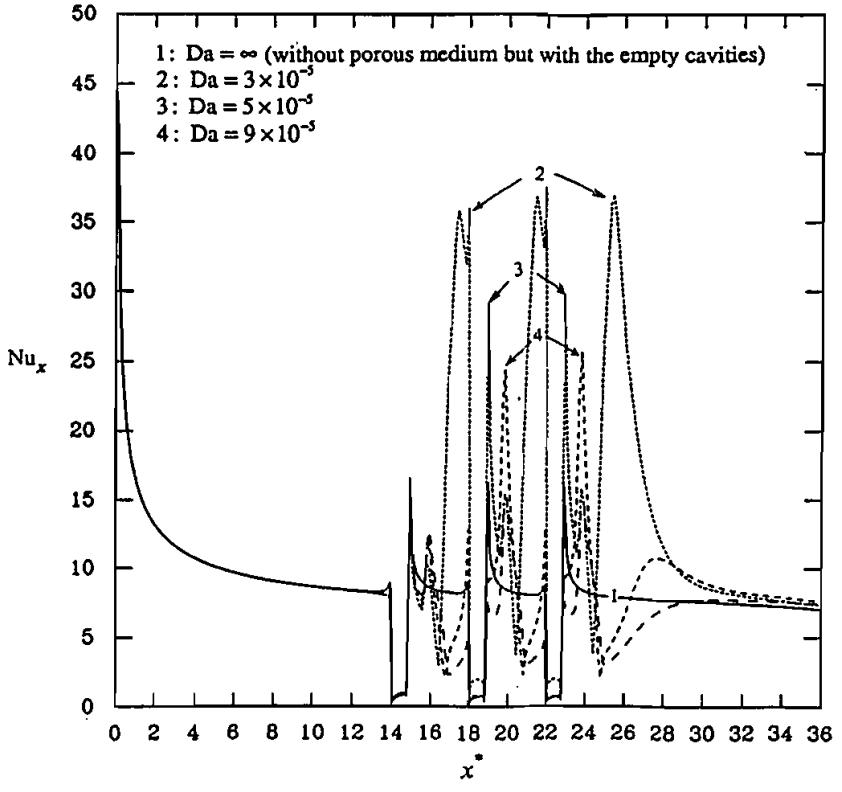

Figure 6. Effects of Darcy number on local Nusselt number distribution for flow in a parallel plate channel with alternate porous cavity–block obstacles on the bottom plate for Re = 750, $\Lambda = 0.35$, Pr = 0.7, $k_{eff}/k_{ff} = 0.1$, $A = 4$, $B = 1$, $H^* = 0.25$.

channel that still includes the empty cavities. As expected, when the Re grows from 750 to 1000, both peak and trough values of Nu_x increase. However, as Re increases further to 1500, the results for both peak and trough values of Nu_x are significantly reduced. The reason for this is that as Re increases to 1500, the circulation zone occupies the whole interblock spacing, which completely separates the core flow from the heated wall, thus reducing the convective heat transfer rate from the wall.

Effects of the Darcy number. The Darcy number, $Da = K/R^2$, is directly related to the permeability of the porous medium. The effect of Da shown in Figures 5 and 6 for Re = 750, $\Lambda = 0.35$, Pr = 0.7, $A = 4$, $B = 1$, and $N = 3$, for $Da = 3 \times 10^{-5}$, 5×10^{-5} and 9×10^{-5}, respectively. It can be seen from Figure 5 that as Da increases, the distortion of streamlines becomes less significant and the height of recirculation behind the porous blocks becomes smaller. The interaction between the vortex inside the cavity and the external flow is found to depend on whether the recirculation zone occupies the whole interblock spacing or not. Note that the vortex inside the first cavity is relatively unaffected by the flow outside the cavity. As expected, the distortion of isotherms in the channel region corresponding to the flow field becomes less noticeable with an increase in Da.

The effect of Da on the local Nusselt number distribution is shown in Figure 6. It can be seen that Da has a significant impact on the variation of Nu_x. The peak of each cycle in the local Nusselt number distribution lowers and moves to the right as Da increases. This is because for the larger Da the accelerated fluid penetrates deeper into the porous block. Comparison of local Nusselt number distribution between the channel with and without porous media shows that for the range of Da investigated (3×10^{-5} to 9×10^{-5}), the heat transfer augmentation increases as Da decreases.

Inertial effects. When Re based on the pore diameter of the porous medium is large, the inertial effects become significant. Figures 7 and 8 illustrate the effect of the inertial parameter on the flow field and heat transfer for Re = 1500, Da = 3×10^{-5}, Pr = 0.7, $A = 4$, and $B = 1$ for $\Lambda = 0.35$, 21, and 35. It can be seen that the strength of the recirculation zone increases as the inertial number increases. Furthermore, for larger inertial numbers the interaction between the vortex inside the interblock cavity and the core flow increases. This is due to the larger bulk frictional resistance that the flow inside the porous block will experience for larger inertial numbers. Therefore, larger values of Λ would lead to a larger blowing effect, which increases the distortion in the streamlines and reduces the penetrating extent of the flow into the porous block. As a direct result of the discussed flow field (Figure 7), the larger the value of Λ, the more noticeable the distortion of the isotherms. As can be seen in Figure 8, for the

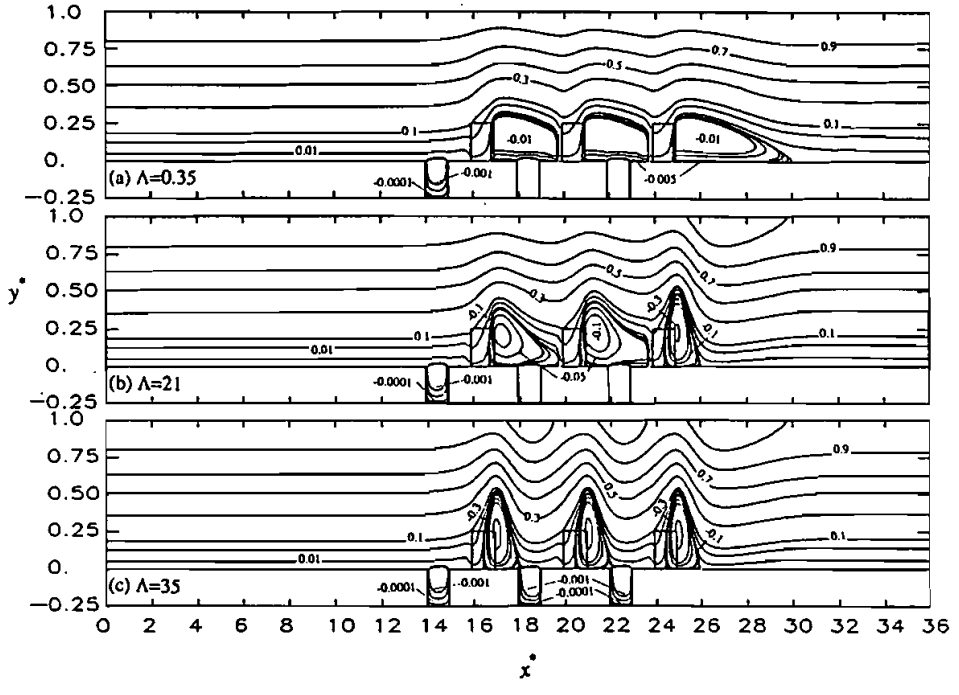

Figure 7. Influence of the inertial parameter on streamlines for flow in a parallel plate channel with alternate porous cavity-block obstacles on the bottom plate for Re = 1500, Da = 3×10^{-5}, $A = 4$, $B = 1$, $H^* = 0.25$.

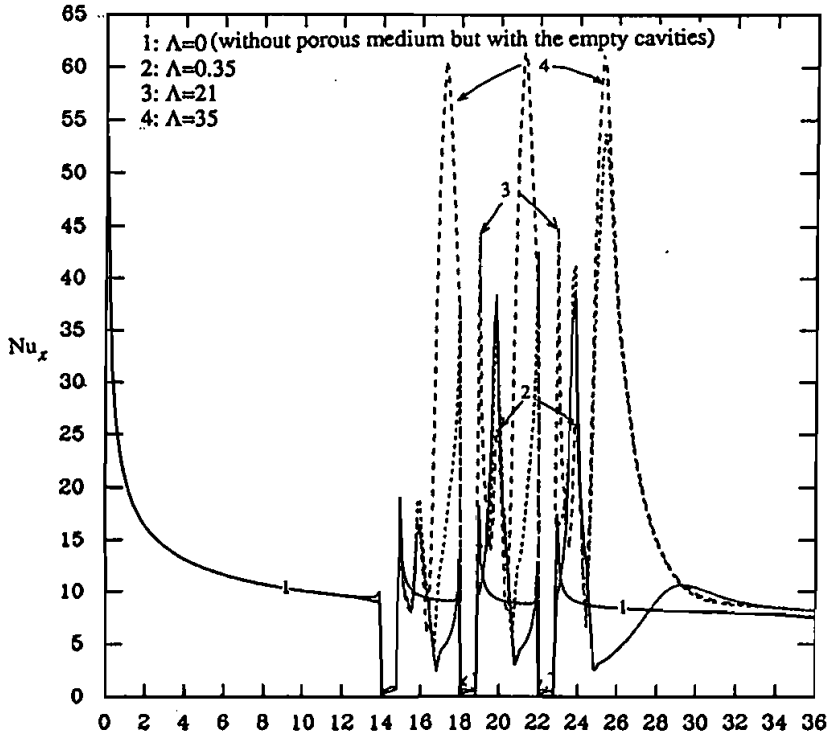

Figure 8. Influence of the inertial parameter on local Nusselt number distribution for flow in a parallel plate channel with alternate porous cavity–block obstacles on the bottom plate for Re = 1500, Da = 3×10^{-5}, Pr = 0.7, $k_{eff}/k_f = 1.0$, $A = 4$, $B = 1$, $H^* = 0.25$.

increase in Λ, the heat transfer augmentation caused by the porous blocks increases.

Prandtl number effects. The Pr effects are shown in Figure 9 for three different Pr for fixed values of Re = 750, Da = 3×10^{-5}, $\Lambda = 0.35$, $A = 4$, and $B = 1$. These values for Pr—0.7 (air), 7.0 (water), and 100 (typical value for oil)—are chosen such that they will cover a wide range of thermophysical properties. Obviously, the variations of Pr have no effect on the flow field, since the values of Re, Da, and Λ are fixed. It was found that increasing Pr in the same flow field decreases the thickness of the thermal boundary layer in the core flow and increases the extent of thermal penetration into the cavity. Due to the lower value of the thermal diffusivity, the temperature gradient is larger for larger Pr. As expected, both peak and trough values of Nu_x increase with an increase of the Pr (Figure 9).

Effect of the geometry of the porous cavity–blocks. The geometric parameters A and B reflect the influence of the aspect ratio of the porous cavity or the block and the interspace between porous cavity and block. The effect of changing the height of the porous block on the flow and temperature fields is depicted in Figure 10. The streamlines for Re = 750, Da = 3×10^{-5}, $\Lambda = 0.35$,

and Pr = 0.7, and for different heights of the porous blocks and different porous-block interspacing are shown in Figure 10. It can be seen that the streamlines get less distorted as the height of the porous block is decreased. In addition, the strength and size of the recirculation regions behind the porous block are lessened significantly for smaller block heights. Also, for smaller porous-block heights the influence of the external core flow on the vortex inside each cavity is diminished, which reduces the thermal penetration into the porous cavity. This is due to the considerable decrease of the blowing effect caused by shorter porous blocks.

Comparison of streamlines in Figure 10 shows that the porous block–cavity interaction decreases as the spacing between the porous block and cavity increases from $B = 1$ to $B = 2$, in which each porous cavity is occupied by a closed vortex. This is a direct result of the increase in the space between the porous block and cavity. The closed vortex inside the cavities leads to a decreased thermal penetration into the porous cavity. Finally, it was also shown that increasing the number of porous cavity–block obstacles had no effect on the flow and heat transfer characteristics that were presented in this work.

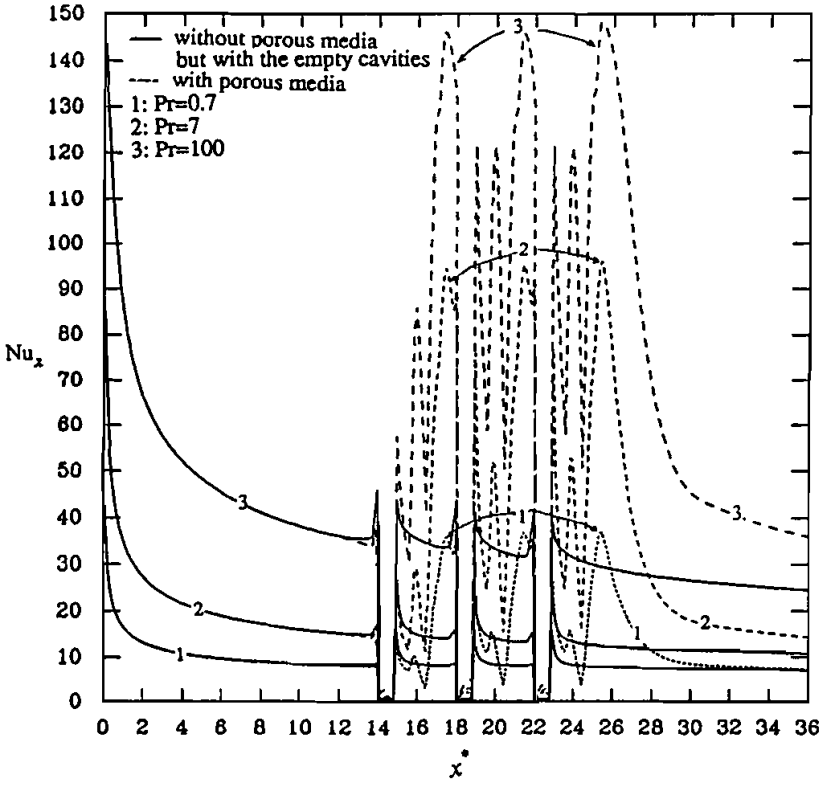

Figure 9. Prandtl number effects on local Nusselt number distribution for flow in a parallel plate channel with alternate porous cavity–block obstacles on the bottom plate for Re = 750, Da = 3×10^{-5}, $\Lambda = 0.35$, $k_{eff}/k_f = 1.0$, $A = 4$, $B = 1$, $H^* = 0.25$.

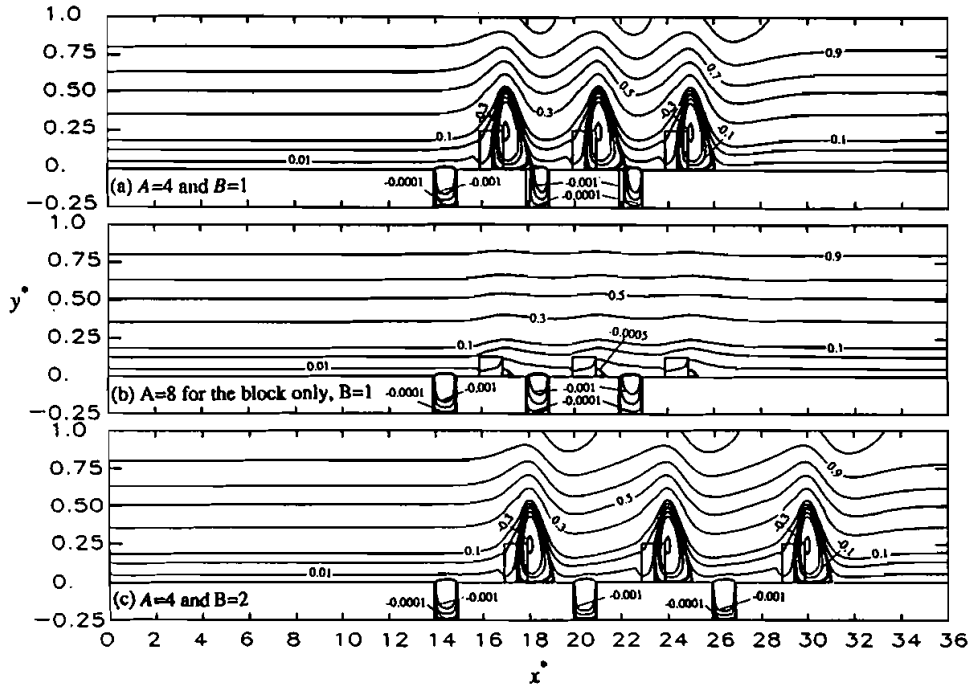

Figure 10. Influence of the geometric parameters A and B on streamline for flow in a parallel plate channel with alternate porous cavity–block obstacles on the bottom plate for Re = 750, Da = 3×10^{-5}, $\Lambda = 0.35$, Pr = 0.7, $k_{eff}/k_f = 1.0$, $B = 1$, $H = 0.25$.

CONCLUSIONS

An investigation of flow and heat transfer in a constant-temperature parallel plate channel with alternate porous cavity and block obstacles on the bottom plate is presented in this work. The analysis for the fluid-saturated porous region is characterized by the Brinkman-Forchheimer-extended Darcy model. The rectangular porous cavities and blocks change the incoming parabolic velocity field significantly, resulting in vortices between the blocks and cavities. It is shown that the porous medium provides a penetrating random structure, which augments the mixing in the fluid and profoundly changes the heat transfer characteristics within the channel. The dependence of flow and temperature characteristics on the governing parameters, such as the Darcy number, the Reynolds number, inertia parameter, the Prandtl number, and two geometric parameters, is documented. The results of this investigation show that the interactions between the vortices residing inside the cavities and the vortices after the porous blocks have a significant effect on the flow and thermal characteristics of the channel.

REFERENCES

1. R. K. Shah and A. L. London, Laminar Flow Forced Convection In Duct, Suppl. 1, in T. F. Irvine and J. P. Hartnett (eds.), *Advances in Heat Transfer*, Academic, San Diego, Calif., 1987.

2. J. C. Y. Koh and R. Colony, Analysis of Cooling Effectiveness for Porous Material in a Coolant Passage, *ASME J. Heat Transfer*, vol. 96, pp. 324–330, 1974.
3. J. C. Y. Koh and R. L. Stevens, Enhancement of Cooling Effectiveness by Porous Material in Coolant Passage, *ASME J. Heat Transfer*, vol. 97, pp. 309–311, 1975.
4. W. M. Rohsenow and J. P. Hartnett, *Handbook of Heat Transfer*, McGraw-Hill, New York, 1973.
5. M. Kaviany, Laminar Flow through a Porous Channel Bounded by Isothermal Parallel Plates, *Int. J. Heat Mass Transfer*, vol. 28, pp. 851–858, 1985.
6. D. Poulikakos and K. Renken, Analysis of Forced Convection in a Duct Filled with Porous Media in Heat Transfer, in *Geophysical and Geothermal System*, *ASME HTD*, vol. 76, pp. 9–20, 1987.
7. D. D. Joseph and L. N. Tao, Lubrication of a Porous Bearing–Stokes' Solution, *J. Appl. Mech.*, pp. 753–760, 1966.
8. G. I. Beavers and D. D. Joseph, Boundary Conditions at a Naturally Permeable Wall, *J. Fluid Mech.*, vol. 30, pp. 197–207, 1967.
9. G. I. Taylor, A Model for the Boundary Condition of a Porous Material—Part I, *J. Fluid Mech.*, vol. 49, pp. 319–326, 1971.
10. S. Richardson, A Model for the Boundary Condition of a Porous Material—Part II, *J. Fluid Mech.*, vol. 49, pp. 327–336, 1971.
11. T. Levy and E. Sanchez-Palencia, On Boundary Conditions for Fluid Flow in Porous Media, *Int. J. Eng. Sci.*, vol. 13, pp. 923–940, 1975.
12. K. Vafai and R. Thiyagaraja, Analysis of Flow and Heat Transfer at the Interface Region of a Porous Medium, *Int. J. Heat Mass Transfer*, vol. 30, pp. 1391–1405, 1987.
13. D. Poulikakos and K. M. Kazmierczak, Forced Convection in a Duct Partially Filled with a Porous Material, *ASME J. Heat Transfer*, vol. 109, pp. 653–662, 1987.
14. K. Vafai and C. L. Tien, Boundary and Inertia Effects on Flow and Heat Transfer in Porous Media, *Int. J. Heat Mass Transfer*, vol. 24, pp. 195–203, 1981.
15. M. Kaviany, Boundary Layer Treatment of Forced Convection Heat Transfer from a Semi-Infinite Flat Plate Embedded in Porous Media, *ASME J. Heat Transfer*, vol. 109, pp. 345–349, 1987.
16. P. J. Roache, *Computational Fluid Dynamics*, Hermosa, Albuquerque, N. Mex., 1982.
17. K. Vafai and S. I. Kim, Analysis of Surface Enhancement by a Porous Substrate, *ASME J. Heat Transfer*, vol. 112, pp. 700–705, 1990.
18. S. B. Sathe, W. Q. Lin, and T. W. Tong, Natural Convection in Enclosures Containing an Insulation with a Permeable Fluid-Porous Interface, *Int. J. Heat Fluid Flow*, vol. 9, pp. 389–395, 1988.
19. K. M. Kelkard and S. V. Patankar, Numerical Prediction of Flow and Heat Transfer in a Parallel Plate Channel with Staggered Fins, *J. Heat Transfer*, vol. 109, pp. 25–30, 1987.
20. J. Adams and J. A. Ortega, A Multicolor SOR Method for Parallel Computation, *Proc. of Int. Conf on Parallel Procession*, pp. 53–56, 1982.
21. D. Greenspan, Numerical Studies of Steady, Viscous, Incompressible Flow in a Channel with a Step, *J. Eng. Math.*, vol. 3, pp. 21–28, 1969.
22. S. V. Patankar, *Numerical Heat Transfer and Fluid Flow*, Hemisphere, Washington, D.C., 1980.
23. T. S. Lundgren, Slow Flow through Stationary Random Beds and Suspensions of Spheres, *J. Fluid Mech.*, vol. 51, pp. 273–299, 1972.
24. G. Neale and W. Nader, Practical Significance of Brinkman's Extension of Darcy's Law Coupled Parallel Flows within a Channel and a Bounding Porous Medium, *Can. J. Chem. Eng.*, vol. 52, pp. 475–478, 1984.